Design and construction of a well-collimated Rubidium effusive oven

A thesis submitted in partial fulfillment of the requirement
for the degree of Bachelor of Science in Physics
from the College of William and Mary in Virginia,

by

Valo J. Dandashi

Advisor: Prof. Seth A. Aubin

Prof. Saskia Mordijck

Williamsburg, Virginia
May 6 2025

Abstract

Well collimated atomic beams are necessary for many atomic experiments where the Doppler effect needs to be suppressed and the atom must be localized in two dimensions. However, atomic beam apparatuses are typically not commercially available for a given element, and so experimenters have to build their own. Further, the design of a given atomic beam source is specific to the particular atom used and the requirements of the research being conducted with those atoms. Here we present the design and construction methods for a well-collimated atomic beam source for rubidium atoms. The design consists of an effusive oven with a heated tube and copper cold cup as collimating components. In addition to design and construction details, this thesis describes the commissioning of the apparatus, including vacuum performance and atomic beam initial characterization.

Contents

List of Figures

List of Tables

Acknowledgments

I would like to thank Seth Aubin for his stellar guidance on this project, without whom none of this would have been possible. His advice throughout my time at William & Mary has been invaluable. Additionally, I would like to thank Saskia Mordijck, who ran our physics senior group therapy excellently while also providing key insights into writing and scientific communication. This project also would not have been possible without advice from Todd Averett and William Henninger. Previous work on this project was also completed by Samuel Turner and Yiyang Ding.

I also want to thank my high school physics teachers, Adam Smith and Mark Hannum, for inspiring me to go down this path, and Rachel Mills for all her advice and support in my senior year. You all cultivated my love for physics, planted the idea of teaching in my mind, and showed me that anyone can be a scientist.

Finally, I would like to thank my parents, for reading through this thesis without understanding a word of it. I would not be where I am today without their support. Thank you to my friends, especially Giselle Boudreaux, Rosemary Raynal, Amelia Magee, Erin Young, Sidney Woloszynowski, Sara Package, and Sebastian Cannito, for being my "general audience" and listening to me yap.

Chapter 1

Introduction

1.1 Motivation

In the field of atomic experimentation, researchers often need a well-collimated beam of atoms. Such a source would, ideally, produce atoms traveling at a small angle, in the same energy level, with no interatomic collisions, and with all atoms carrying the same spin. Furthermore, each individual atom emitted by the atomic source would be nearly identical to every other emitted atom, leading to greater predictability in experimental environments. The reduction of variability and error in the emitted atoms allows for more accurate modeling of a given experiment ahead of time, and the reduction of variables allows physicists to learn more from their experiment.

Three specific experimental benefits of an atomic beam are the localization of the atoms in two dimensions, the suppression of the Doppler effect, and the ability to sequence experimental actions spatially rather than temporally (See Figure 1.1). By the nature of the atoms traveling as a well-collimated beam, the atoms are highly localized in the two dimensions forming a plane transverse to the atomic motion. This localization applies to the velocity of the atoms as well. Velocity localization in a transverse plane to the motion of the atoms suppresses the Doppler effect in this plane, as it is dependent on the cosine of the angle between an incident wave and

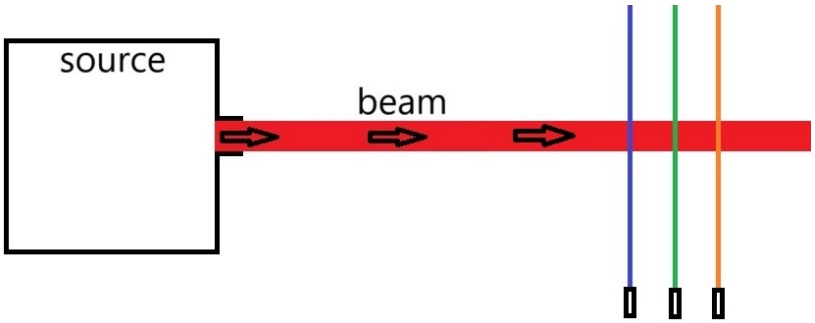

Figure 1.1: An idealized example of an atomic beam with perfect collimation, with spatially separaetd experimental components demonstrating the Doppler Effect. The multicolored lasers (right) are orthogonal to the atomic beam (represented in red).

atomic velocity. With velocity in a single direction and incident waves transverse to that direction, this angle is ideally 90° and the cosine of the angle is 0, eliminating the Doppler effect. Finally, the traveling nature of the atomic beam allows for the conversion of temporal sequences experimental components, such as a laser pulse, to spatial sequences. As an atom passes through a given experimental action, it is both able to exit the location of influence and is replaced by another atom traveling behind it, allowing for continuous use of experimental components that otherwise would need to be timed to allow pulsing action or re-cooling of atoms. This reduces the engineering burden on experimental design; for instance, a laser that would need to be temporally pulsed when used on an atomic chip may be replaced by a continuous wave laser directed perpendicular to the atomic beam.

In the context of ultracold atom experiments, including ultracold atom interferometry, an atomic beam can serve as an effective source for a Zeeman slower. A Zeeman slower, in turn, may be used as a high-flux source of cold atoms for a magneto-optical trap (MOT). Such Zeeman slower-based apparatuses can operate at a high repetition rate for generating samples of ultracold atoms and quantum gases. This is in contrast to alternate methods for sourcing atoms for a magneto-optical trap, such as drilling a hole in a mirror forming the MOT or using a pushing beam, which can destabilize

the MOT while failing to collimate the beam as precisely as desired [1].

1.2 Atomic Beam Sources

The earliest atomic beam sources, beginning in the early 1900s, were composed of an effusive oven: a chamber of atomic material heated to a vapor and allowed to pass through a small orifice in the chamber to another chamber held in vacuum [2]. The size of the orifice and the temperature to which the atoms are heated control the rate at which the atoms emerge, as seen in Section 2.1. However, the beam produced by such an oven (or Knudsen cell) is of poor quality. The atoms emerge at a wide angle relative to the hole, resulting in wasted material and less predictable atoms. This wasted material necessitates more frequent reloading of the chamber with material, while also poisoning the vacuum components as they are covered in atoms from the oven instead of being primarily directed to the experimental structures.

There have been historic attempts to address this wide angle, namely by using gas dynamic expansion through a nozzle as opposed to free gaseous effusion [2]. These early attempts at collimation, while effective, have limited applicability when compared to a traditional effusive oven with an additional collimating apparatus. Attempts to collimate the beam emerging from the effusive oven have yielded positive results, and recent research in the field has produced sturdy, compact beam sources that can be easily reloaded without breaking vacuum. Bell *et al.* created a design in 2010 for a rubidium effusive oven with a collimation mechanism and a 3-ft Zeeman slower, in conjunction with Lin *et al.* in 2009 [3, 4]. Wouters *et al.* then modified these past designs in 2016 for an apparatus that was more compact and optimized for their specific experimental purposes [5]. The basic structure of these beam designs remains broadly identical, and it is the basis of our design as well.

In this basic structure, the beam is generated in vacuum by a series of individual

components that connect into one another: an effusive oven, a collimation tube, and a copper cold cup, leading into another pumping tube that directs the generated beam to the experimental apparatus (e.g. a Zeeman slower, a magneto-optical trap, etc.). The effusive oven consists of an ampule of atomic material heated to a vapor [2]. In the case of rubidium, heating the ampule to 80 °C is sufficient. The collimation tube is a long, thin tube, heated to approximately 120 °C, that limits the incident angle of the atoms upon exiting the system from the wide incident angle generated by the Knudsen cell. Finally, the cold cup, cooled to -30 °C, "catches" any atoms that emerge from the collimation tube at a wide incident angle by rapidly reducing their temperature upon impact, which captures the rogue atoms and prevents them from traveling to the downstream experimental section of the apparatus where they could contaminate the vacuum.

1.3 Thesis Structure

This thesis reports on the successful design and construction of a rubidium atomic beam apparatus. The apparatus is being commissioned and is currently operating at a vacuum pressure of $2 \cdot 10^{-5}$ Torr. The beam is not yet fully operational, but tests of its individual components indicate that it may be activated once the appropriate vacuum pressure (on the order of 10^{-7} Torr) has been achieved. The thesis is structured in the following manner: Chapter 2 reviews the basic theory of atomic beams. Chapter 3 presents the design, assembly methods, and complications in assembly of the beam as it exists today. Chapter 4 discusses the testing of individual components of the beam apparatus. Chapter 5 concludes that while further testing may be needed on certain components and outgassing/bake-out procedures will likely be necessary to improve the vacuum pressure within the apparatus, the components and structure are largely working as intended and the beam will be functional in the near future.

Chapter 2

Kinetic Gas Theory

The behavior of atoms within a single-channel effusive oven is governed by kinetic gas theory. In particular, net flux and angular distribution of the effusing molecules are two of the relevant beam characteristics that may be verified experimentally [2]. This chapter reviews the basic physics of effusive ovens, their collimation, and their reduction of Doppler broadening, as well as considerations regarding the use of rubidium.

2.1 Effusive Ovens

A traditional Knudsen cell involves heating a material to sublimation in a low pressure environment, then allowing the atomic vapor to effuse through a small orifice in the cell [5]. The net flux Φ (atoms/s) of a Knudsen cell with gas density n in atoms/m^2 and orifice radius r is given by

$$\Phi = \frac{1}{4} n \pi r^2 \bar{v}, \tag{2.1}$$

where $\bar{v}$ is the average speed of the gas in the cell [2]. This average speed is given by

$$\bar{v} = \sqrt{\frac{8 k_B T}{\pi m}}, \tag{2.2}$$

with k_B Bolztmann's constant, T the temperature of the cell, and m the atomic mass of the material within the cell. For a rubidium vapor above its melting point, the

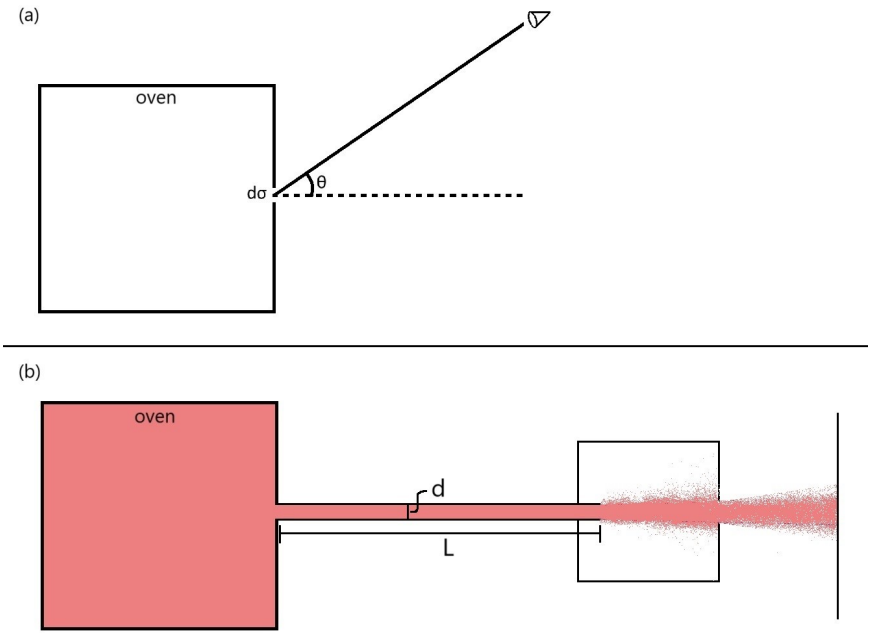

Figure 2.1: Angular distributions of particles effusing from the oven. (a) Effusive oven with no collimation. $d\sigma$ is the oven orifice and θ is measured from the normal axis to $d\sigma$. (b) Effusive oven with collimation tube and cold cup. Only particles within the blue lines contribute to the net flux of the apparatus.

atomic density depends on temperature and can be approximated by

$$n(T) = p^* \frac{e^{-T^*/T}}{k_B T}, \tag{2.3}$$

where $p^* = 2.05 \cdot 10^9$ Pa and $T^* = 9.30 \cdot 10^3$ K are the pressure and temperature constants, respectively, for the vapor pressure of solid rubidium [5, 2, 6, 7]. With no collimation, the angular distribution of the effusive molecules is

$$\frac{dN}{dt} = I(\theta) = \frac{1}{4\pi} n\bar{v}\sigma \cos(\theta), \tag{2.4}$$

where σ is the area of the orifice and θ is the angle from the normal vector of $d\sigma$ (See Figure 2.1(a)). Collimation, in this case via a long thin tube, impacts $I(\theta)$ by narrowing the spread of the atoms.

2.2 Collimation

When an effusive oven is connected to a long, thin tube of length L and diameter d (see Figure 2.1b), the behavior of the atoms effusing through the tube is dependent on the Knudsen number $K_{n,x} = \frac{\Lambda}{x}$, where Λ is the mean free path within the tube, and x is L or d depending on if the collision scheme being examined is along or across the tube, respectively. Here,

$$\Lambda = (4\sqrt{2}\pi r_{vdw}^2 n(T))^{-1}, \tag{2.5}$$

where r_{vdw} is the Van der Waals radius of the particle; for rubidium, $r_{vdw} = 303$ pm [5]. The behavior of the effusing particles falls into one of three categories, dependent on the values of $K_{n,d}$ and $K_{n,L}$. These three categories — labelled transparent, opaque, and continuum by H. Pauly in *Atomic and Molecular Beam Methods* — are characterized by the interatomic collisions allowable by the dimensions of the system: in the transparent regime ($K_{n,d} > 1$, $K_{n,L} > 10$), no collisions are possible between atoms within the tube; in the opaque regime ($K_{n,d} > 1$, $K_{n,L} < 10$), collisions occur for atoms moving axially along the tube, but not across it; in the continuum regime ($K_{n,d} < 1$, $K_{n,L} < 10$), collisions occur both along and across the tube [5, 2]. The latter is comparable to the behavior of fluids and gases in a room.

Wouters *et al.* found that with a tube following the dimensions inner diameter 2 mm and length $L = 95$ mm heated to 120 °C, as in this design, the atomic behavior follows the opaque mode of operation [5]. In particular, $\Lambda = 0.0304$ m, giving Knudsen numbers $K_{n,d} = 15.217$ and $K_{n,L} = 0.320$. In this regime, the angular distribution of atoms emerging from the tube is broad relative to that of the transparent regime while still narrowed from the base effusive oven distribution, and net flux is not impacted. The full angular distribution for this scheme is not available analytically; however, there are analytical expressions that the distribution must follow, which are expressed

by H. Pauly in *Atomic and Molecular Beam Methods* [2].

An additional collimation factor can be provided by a copper cold cup, which has an aperture opposite the effusive end of the collimation tube (see Figure 2.1b). This copper box is cooled to cause rubidium that effuses at a broad angle to stick to the sides of the wall, protecting downstream vacuum components from rogue atoms that can contaminate the vacuum quality [8]. As such, the addition of the cold cup helps to limit the broadened spread of atoms by catching atoms that effuse at a broader angle than desired (See Figure 2.1(b)).

2.3 Doppler Effect

There are two primary sources of motivation for collimating an atomic beam source. The first, as described in Section 1.2, centers on predictability of the emergent atoms and minimizing wasted material. The second rests on the phenomenon of the Doppler effect, or the stretching and compressing of waves based on the relative motion of the involved reference frames. The effect is characterized by the change Δf in wave frequency

$$\Delta f = \frac{\vec{k} \cdot \vec{v}}{2\pi}, \tag{2.6}$$

where $\vec{k} = \frac{2\pi}{\lambda}\hat{n}$ is the wave vector for an incident wave with wavelength λ and propagation direction $\hat{n}$, and $\vec{v}$ is the velocity of the "observer." For the purposes of laser interaction with atoms in a beam, the observer is an arbitrary atom within the the beam, and $\vec{v}$ is the velocity of that atom. In Figure 1.1, the vertical lasers correspond with $\vec{k}$ in Equation 2.6, while $\vec{v}$ is the velocity of the atoms composing the red atom beam. In this case, $\Delta f = 0$ since the beam and lasers are orthogonal to one another.

The primary manifestation of the Doppler effect in laser-based experiments is the broadening of spectral lines (see Figure 2.2), which can obscure the fine structure that, often, is being studied. In a well-collimated atomic beam, all atoms have iden-

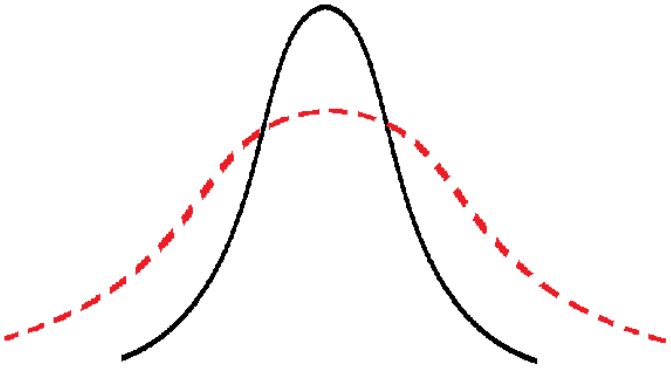

Figure 2.2: Example of the Doppler broadening effect on spectral lines. The black line represents the original waveform, while the red dashed line represents the waveform being measured under a Doppler effect.

tical velocities, and therefore the Doppler effect can be eliminated by aligning the experimental components to be orthogonal to the velocity of the atoms in the beam. This elimination of the Doppler effect is a desirable trait of well-collimated beams, as it removes the aforementioned spectral broadening and allows for more precise measurement.

For rubidium atoms at $T = 100$ °C, Equation 2.2 gives the average speed as

$$\bar{v} = \sqrt{\frac{8 \cdot 1.381 \cdot 10^{-23} \text{ J K}^{-1} \cdot 373.15 \text{ K}}{\pi \cdot 87 \text{ amu}}} = 301.436 \frac{\text{m}}{\text{s}}. \tag{2.7}$$

Then, by Equation 2.6, Δf by a laser with wavelength 780 nm and maximal incident angle 90° is

$$\Delta f = \frac{2\pi \cdot 301.436 \frac{\text{m}}{\text{s}}}{2\pi \cdot 780 \cdot 10^{-9} \text{ m}} = 386.456 \text{ MHz}. \tag{2.8}$$

As the rubidium atoms in this atomic beam source are heated to 80 °C and 120 °C in different areas of the apparatus, $\bar{v} = 301.436 \frac{\text{m}}{\text{s}}$ is a reasonable estimation for the average speed of the atoms present within the beam.

2.4 Use of Rubidium

Rubidium is a highly versatile atom due to its low melting point and status as an alkali metal, which can be easily laser cooled. However, as alkali metals are relatively reactive, their usage can have adverse effects on the materials composing an apparatus. As indicated by Ma *et al.* in 2009 and Gádoros *et al.* in 2022, rubidium vapor can chemically impact glass components upon long exposure [9, 10]. However, these impacts can vary depending on the composition of the glass used. As Ma *et al.* found, Pyrex glass absorbs the equivalent of 6 to 7 monolayers of liquid rubidium, which can be removed by directly heating the glass surface until the rubidium re-vaporizes [9]. Gádoros *et al.* found that sections of both condensed rubidium and rubidium silicate had formed on their quartz glass optical window [10]. Both types of material were able to be removed using laser interaction. These results indicate that while rubidium-glass interactions are minimal and non-permanent, as opposed to those of other alkali metals, any optical windows are recommended to be either Pyrex glass, which allows for easy internal cleaning, or sapphire glass, which has no interaction with any alkali metal vapor. For cost and time-efficiency, Pyrex glass optical windows are used for this design.

2.5 Summary

Through collimation and use of a cold cup, the angular flux distribution of an effusive oven may be narrowed to the point that the effusing atoms primarily travel in the same direction as one another. This, in turn, allows for the elimination of the Doppler effect by placing electromagnetic experimental components orthogonal to the path of the beam. Elimination or reduction of the Doppler effect leads to the emergence of fine structure in the measurable spectral data of the atoms within the beam, a highly

desirable outcome for use of the beam as part of larger experimentation. Rubidium in specific is useful as the atom present in the beam due to its status as an alkali metal and behavior akin to a two-level atom. The detrimental impacts of using rubidium in a vacuum apparatus may be accounted for by using specific materials, namely Pyrex or sapphire glass.

Chapter 3

Design and Assembly Methods

As described in Section 1.2, the atomic beam source design is largely based on past work by Bell *et al.*, Wouters *et al.*, and Lin *et al* [3, 5, 4]. Additionally, previous work was done at William & Mary on this project by Samuel Turner and Yiyang Ding to determine preliminary assembly methods [11, 12]. Physical assembly of the system also composed a significant amount of the work for the thesis research.

3.1 Atomic Beam Source Design

A schematic of the design for the beam chamber can be seen in Figure 3.1. Beginning at the bottom left of Figure 3.1, a glass ampule containing rubidium is loaded into the stainless steel bellows (A). The bellows may be flexed to break the ampule and release the rubidium into the system. The bellows are heated to approximately 80 °C, allowing the rubidium to partially pass into a vapor state.

The bellows is attached to a collimation tube (D) using a T-connector (B), oriented so the unused end is aligned with the tube. This allows for a visual check of alignment prior to the sealing of the system for vacuum. The T-connector is also heated to approximately 80 °C. The collimation tube has inner radius 1 mm, outer radius 2 mm, and length 10 mm, which aligns with the tube used by Wouters *et al.* [5]. The tube is suspended within a spacer component (C) that also serves as a transition

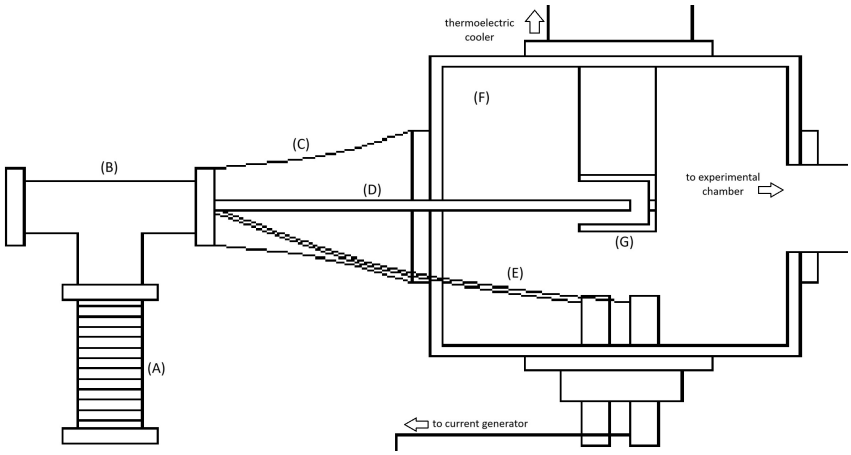

Figure 3.1: Design schematic for the atomic beam source. This version features the tapered spacer (C) from V2.0 of the beam source. Not to scale.

from the smaller flange diameter (1.33") to the larger (2.75"). The open end of the tube is suspended within a copper cold cup (G) (schematic in Figures 3.2), which will eventually be cooled externally to -30 °C by a thermoelectric cooling system connected to a copper rod with diameter 0.9 cm. The assembly of the collimation tube with the copper cold cup and copper rod may be found in Figure 3.4. The opposite flange of the main chamber leads into the experimental chamber (H).

The original cold cup design features a "vertical" screw orientation, as seen in Figure 3.2a. Complications during manufacturing led to the screw holes needing to be closer together than originally intended to allow for appropriate clearance of the drill bit with the walls of the cold cup. As a result, a second cold cup design (Figure 3.2b) was created with minor modifications, namely setting the screw holes at a diagonal. This allows for a larger distance between the holes, which adds greater stability to the assembly while still keeping the appropriate clearance. As such, there are two versions of the cold cup: one with the original screw locations and one with the modified screw locations. Both cold cups may be seen in Figure 3.3. The version with modified screw locations is used in the final apparatus.

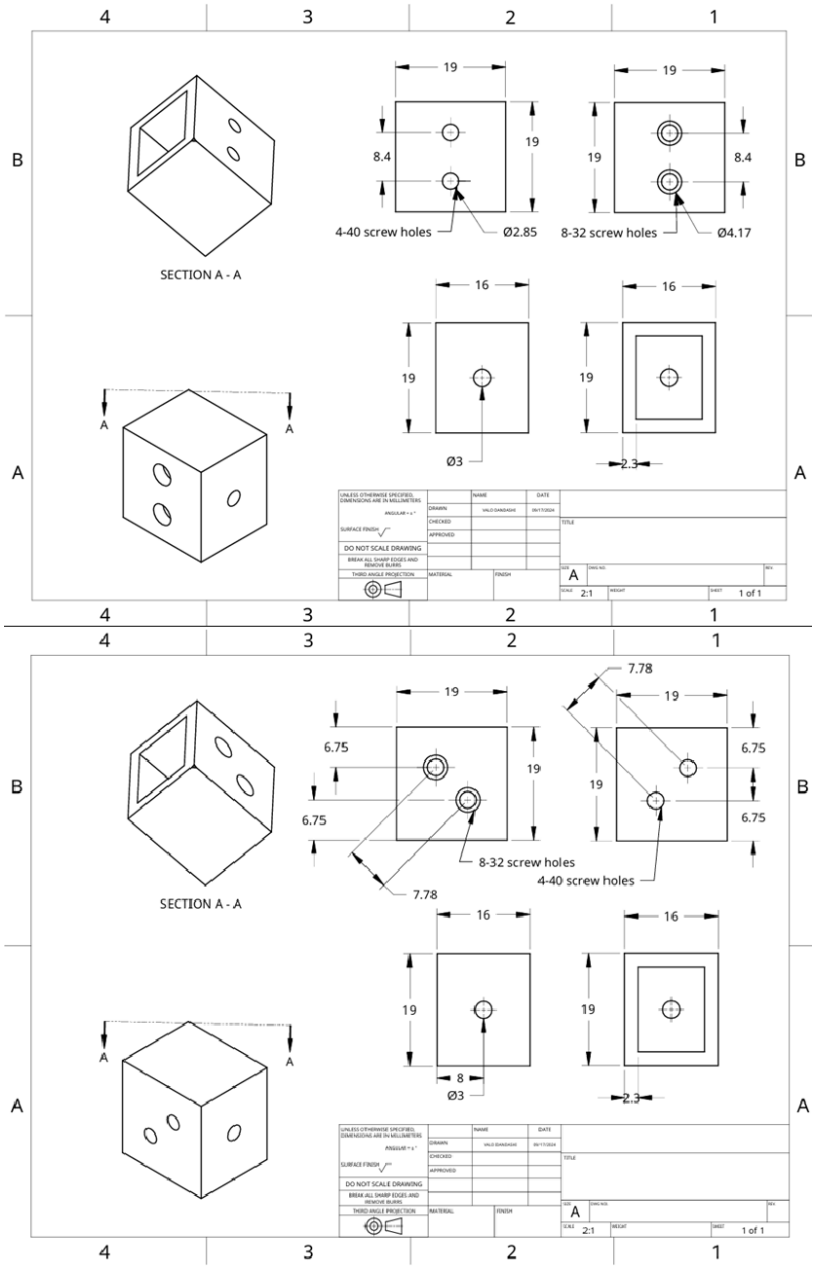

Figure 3.2: (a) (Top) Schematic design for the copper cold cup. The two 4-40 screw holes align with the 4-40 screw holes in the copper rod to attach the pieces together (See Figure 3.4). The 8-32 screw holes are present to allow a screwdriver into the cold cup to screw together the cold cup and rod, and are threaded so they can be plugged. The collimation tube is suspended in the open side of the cold cup, while the beam emerges from the hole in the opposite side. (b) (Bottom) Altered schematic design for the copper cold cup. The screw holes are set at a diagonal to allow for a larger distance between screws than possible in the original cold cup design.

Figure 3.3: The completed copper cold cups, with screws inserted into the threaded holes. (L) V2.0 cold cup, with the diagonal screw holes on display. (R) V1.0 cold cup, with vertical screw holes on display.

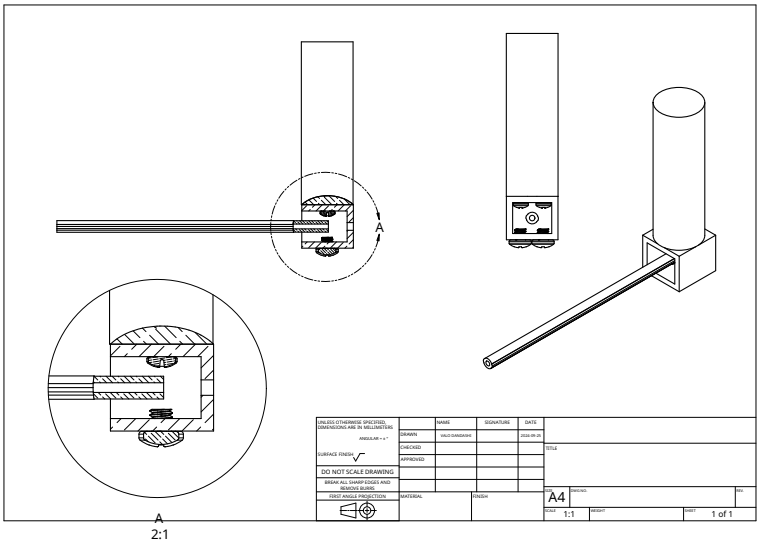

Figure 3.4: Assembly drawing for the copper cold cup, copper rod, and collimation tube. The non-pictured end of the copper rod emerges from the vacuum chamber and is cooled with a thermoelectric system. This assembly drawing was created using the original (V1.0) copper cold cup design seen in Figure 3.2a, but the assembly is identical with the modified V2.0 design in Figure 3.2b. Cutout A: Cross-section of the assembly within the cold cup.

Component	Manufacturer	Detail	Flange Size
Blank	MCD MFG Inc.	x2	1.33”
Bellows	MCD MFG Inc.	–	1.33”
T-Connector	MCD MFG Inc.	–	1.33”
Tube	McMASTER-CARR	Welded to a spacer flange.	1.33”
Spacer Flanges[1]	MCD MFG Inc.	x4	1.33”
Tapered Spacer[2]	MCD MFG Inc.	–	1.33”/2.75”
1-Inch Spacer	MCD MFG INc.	–	2.75”
34AWG Kapton-Insulated Cu Wire	Accu-Glass Products	PN110824	–
High-Temp UHV connector epoxy	Accu-Glass Products	PN111785	–
Cu Gaskets	–	x6	1.33”
UHV Cube	MCD MFG Inc.	–	2.75”
Cu Rod	–	2 4-40 holes	2.75”
Cu Cold Cup	–	See Figure 3.2	–
Electrical feedthrough	MCD MFG Inc.	–	2.75”
Ceramic Standoff	Accu-Glass Products	.5”	–
Angle Valve	Nor-Cal Products	–	2.75”
HiPace 1800 Pump	Pfeiffer Vacuum	–	3.375”
T-Connector	Huntington Labs	–	2.75”
2.5-Inch Bellows	Varian	–	2.75”
Elbow	Huntington Labs	–	2.75”
5-Inch Nipple	–	–	2.75”
Tapered Nipple	MCD MFG Inc.	–	2.75”/3.375”
Viewport	MCD MFG Inc.	Pyrex glass	2.75”
4-Inch Nipple	Balzers	–	2.75”
Gate Valve	HVA	–	2.75”

Table 3.1: A complete list of components used in the atomic beam source. All components are stainless steel unless otherwise specified. [1]All 4 spacer flanges are used only in the V1.0 Design. A single spacer flange is welded to the tube for the V2.0 design. [2]The tapered spacer is only in the V2.0 Design.

All components are connected using ConFlat flanges, with diameter either 1.33” or 2.75”. A full list of components for the beam chamber, including which component uses which flange size, may be found in Table 3.1. The entire system is held under vacuum, at approximately 10^{-6} Torr, by a vacuum pump connected to the main

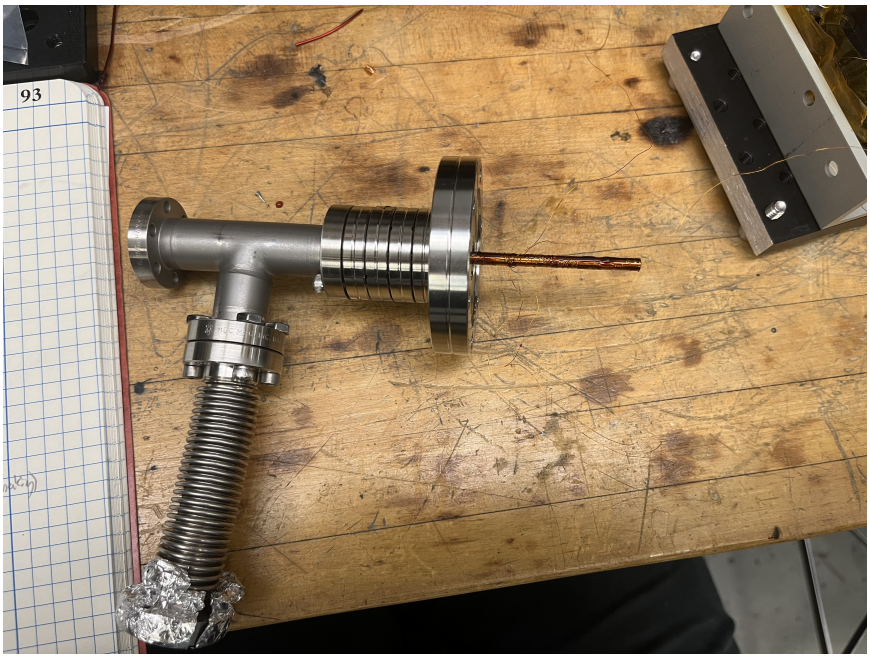

Figure 3.5: Partial assembly of the beam source, completed on 11/20/2024. The bellows, T-connector, and tube with the spacing component are present.

chamber, labeled F in Figure 3.1 and UHV Cube in Table 3.1.

3.2 Assembly Methods

The tube is heated to approximately 120 °C via current run through a 34-AWG Kapton-insulated copper wire (E) (See Table 3.1), wrapped by hand as a double helix (See Figure 3.6) around the tube. This is to avoid a solenoid-induced magnetic field inside the tube by essentially having two solenoids overlapping one another with

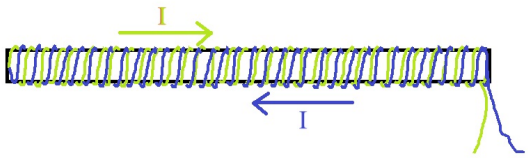

Figure 3.6: Drawing of the double helix wire wrapping method. The green (lighter) and blue (darker) lines represent the sections of wire with current traveling in opposing directions. Both ends of the wire emerge from the right-hand side of the tube.

Figure 3.7: Tapered spacer block for V2.0 atomic beam source.

current traveling in opposing directions, thus canceling out the induced magnetic field. The wire is secured to the tube with UHV-grade epoxy (see Table 3.1), rated for use up to 250 °C, cured for 30 minutes at 90 °C. Two atomic beam sources were initially planned, one with a spacer composed of three 1.33" flanges and one 2.75" flange (V1.0, pictured in Figure 3.5) and the other with a single-piece tapered spacer (V2.0, pictured in Figure 3.7). The assembled beam source contains the V1.0 spacers.

Additionally, two disconnected lengths of wire are used in both of the final collimation tube components due to complications that arose while wrapping the wire. Since the wire sections were different lengths, it is expected that they have different resistances to one another. Therefore, to ensure the same current in both sections on each tube, the wires are placed in series with one another. This is achieved using a ceramic standoff attached to the inside of the electrical feed-through (See Figure 3.8).

The original tapped screw holes on the copper rod are drilled in the wrong location relative to the flange bolt holes due to a failure in communication between the author

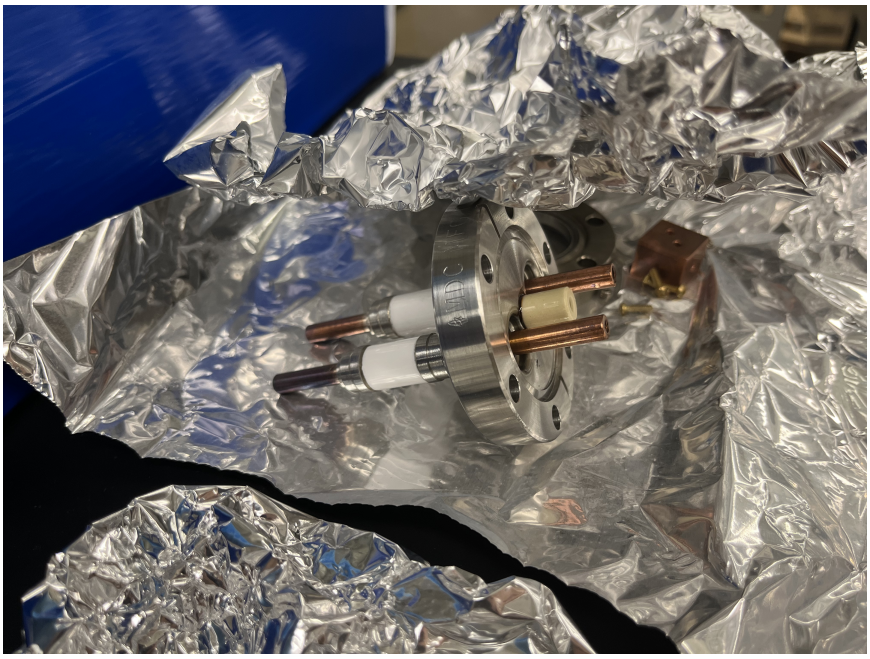

Figure 3.8: Electrical feed-through component with attached ceramic standoff. The standoff is attached directly to the feed-through flange using UHV-rated epoxy.

and the Physics department's machinist. The final version of the rod features two sets of holes as a result, with four holes in total. The "correct" set has a filed groove running through both the holes and the center of the rod's face, while each hole in the "incorrect" set has a groove running to the outside of the rod's face and not intersecting the center. These grooves also serve to outgas the screw holes once the cold cup-rod assembly is placed in vacuum, as otherwise air molecules would be trapped between two smooth surfaces with little space to travel. A mock-up of the circular face of the copper rod may be seen in Figure 3.9.

All components are prepared for vacuum using a three-step washing-and-drying procedure, to ensure heavy oils and contaminants, like those left by a human hand, do not negatively impact the vacuum pressure once pumping begins. Components are washed by hand using Alconox lab-grade dry soap and tap water, then rinsed with distilled water. After air drying, they are soaked in acetone for a minimum of 30 min-

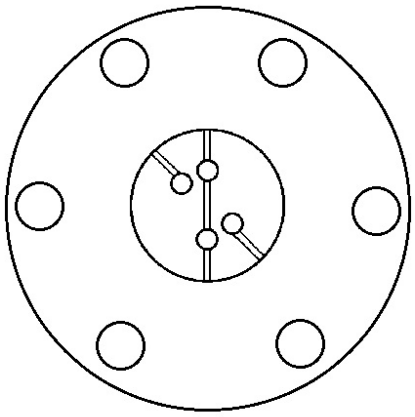

Figure 3.9: A mock-up of the circular face of the copper rod. The outer circle and 6 surrounding smaller circles represent the orientation of the 2.75" CF flange and its 6 bored bolt holes, while the inner circle represents the rod itself. One set of screw holes is vertically oriented and in line with the rotational symmetry of the flange holes, while the other set is misaligned with the flange holes. The straight lines through the screw holes indicate the placement of the filed grooves for outgassing.

utes and air dried, then soaked in methanol for a minimum of 30 additional minutes and left to air dry further. Due to limitations of available containers, larger components were soaked in multiple stages to ensure all areas were thoroughly cleaned. While the time spent partially submerged for each component totalled a minimum of 30 minutes, every section was submerged for a minimum of 10 minutes before the component was rotated to submerge a different area. Sections were overlapping, allowing for a total length of submersion of approximately 15 to 20 minutes for each surface. This piecemeal washing may be a source for poor initial vacuum results in Section 4.2.

Components are attached to one another using a copper gasket and an appropriate number of screws or bolts per connection, that being six for the 1.33" and 2.75" flanges and eight for 4.5" flanges. The screws and bolts must be tightened in a star-like pattern to allow for even molding of the gasket, resulting in a near-leak-free seal.

3.3 Collimation Tube Temperature Measurement

During assembly, the wire must be tested and the epoxy outgassed by applying gradually increasing current. These heat tests serve to ensure that the wire and feedthrough are working as expected before the system is placed under vacuum. Outgassing is necessary because when heated, the epoxy both changes color and produces a strong smell, indicating there are molecules being released when it is heated that would otherwise interfere with the vacuum quality. It also ensures that future calculations of temperature are accurate, as invasive means of measuring tube temperature, such as a thermocouple, cannot be used in vacuum and a thermal camera cannot detect temperature through a window. This means that temperature must be measured by other methods once the system is sealed, namely from calculating the resistance. In the case of the V1.0 tube tests, the temperature is measured using a thermal camera to avoid contact with vacuum components. Comparatively, tube temperature may also be calculated as

$$T = \frac{1}{\alpha}(\frac{R}{R_{ref}} - 1) + T_{ref}, \tag{3.1}$$

where $\alpha = 0.00393\ ^{\circ}C^{-1}$ is the temperature coefficient of copper at T_{ref}; R is the resistance, found using Ohm's Law,

$$V = IR$$

and measured values for voltage (V) and current (I); $T_{ref} = 20\ ^{\circ}\text{C}$; and R_{ref} is calculated using the resistivity of copper. Specifically,

$$R_{ref} = \frac{\rho L}{A} = 6.568\ \Omega, \tag{3.2}$$

where $\rho = 1.724 \cdot 10^{-8}\ \Omega$ is the resistivity of copper, $L = 25$ ft is the approximate length of wire, and $A = 0.02\ \text{m}^2$ is the cross-sectional area for 34AWG wire. The

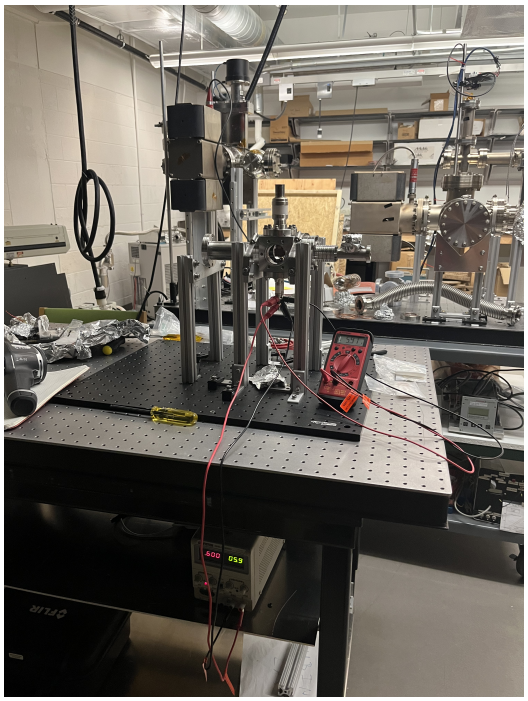

Figure 3.10: Full experimental setup for the preliminary temperature measurements. A GW Instek GPS 3030DD laboratory DC power supply is connected to the electrical feed-through via alligator and banana clips. The feed-through is in turn connected to the 34AWG wire wrapped around the collimation tube and secured with UHV epoxy.

setup for these measurements may be seen in Figure 3.10 and consists of a current generator and multimeter attached using alligator clips to the electrical feed-through.

Preliminary tests of temperature distribution, wire wrapping method, and epoxy application were also performed on a spare length of tube, henceforth referred to as "V0.0," prior to main assembly of the components used in the final beam source. The author used V0.0 to determine the thermoelectric behavior of the tube, wire, and epoxy when the wire is heated with current. The setup for these measurements may be seen in Figure 3.11. Temperature in this case was measured using a type K thermocouple and a multimeter.

The atomic beam source, with design as described in this chapter, was fully assembled as of 14 April 2025 with a gate valve separating the beam source chamber

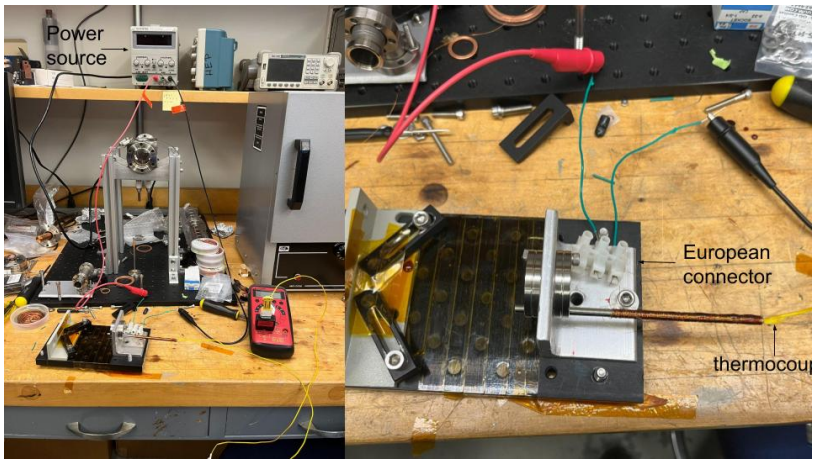

Figure 3.11: (Left) Full experimental setup for the V0.0 temperature measurements. The thick red and black wires are connected to a GW Instek GPS 3030DD laboratory DC power supply using alligator and banana clips. (Right) Close-up on V0.0 tube. The wire wrapped around the tube is soldered to itself and converted to a thicker wire using a European connector. A thermocouple is inserted into the open end of the tube.

from the eventual location of an experimental chamber (labelled in Figure 3.1). An experimental chamber was then completed and incorporated into the vacuum pump-down on 21 April 2025. This chamber consisted of a 2.75" flange six-way cross and features 4 viewports and a blank flange, with the sixth side of the cross connected to the gate valve. One viewport is placed opposite the gate valve to allow for buildup of rubidium over time, providing a visual check of the angular distribution of the beam. Two viewports are placed opposite one another to allow for a laser to cross the atomic beam horizontally. The final viewport is opposite the blank flange and may be used for a photodiode, in order to detect the spectral emissions of the rubidium caused by interaction with the laser. The system has been under continuous vacuum pumping for eight days and has achieved a minimum pressure of $1.23 \cdot 10^{-5}$ Torr. Further aspects of the current status of the apparatus are discussed in Section 4.2.

Chapter 4

Results

The data gathered regarding the completed apparatus primarily centers around the temperature distribution of the collimation tube under different currents and the vacuum pressure achieved when pumping down the system. Due to vacuum leaks and significant delays, discussed in Sections 4.2 and 5.1, a full analysis of the beam characteristics was not possible. However, the results discussed in this chapter have useful information regarding further iterations of the beam design and future improvements on the vacuum pressure within the apparatus.

4.1 Temperature Distribution

Figure 4.1 displays measurements of current and temperature taken for the V0.0 tube on 31 October 2024 and 1, 12, 14, and 15 November 2024. Figure 4.1 also displays resistance calculated using voltage measurements taken on 31 October and 1 and 12 November 2024. The data is labeled by date because there were no meaningful changes in data collection. Variations in value between different days is likely due to different forms of human error, and the fact that the data behaves consistently as current increases within each day supports this assertion. Variation in measured values is due to three predominant factors. First, because of variations in both the wire spacing and the thickness of the epoxy along the length of the tube, temperature

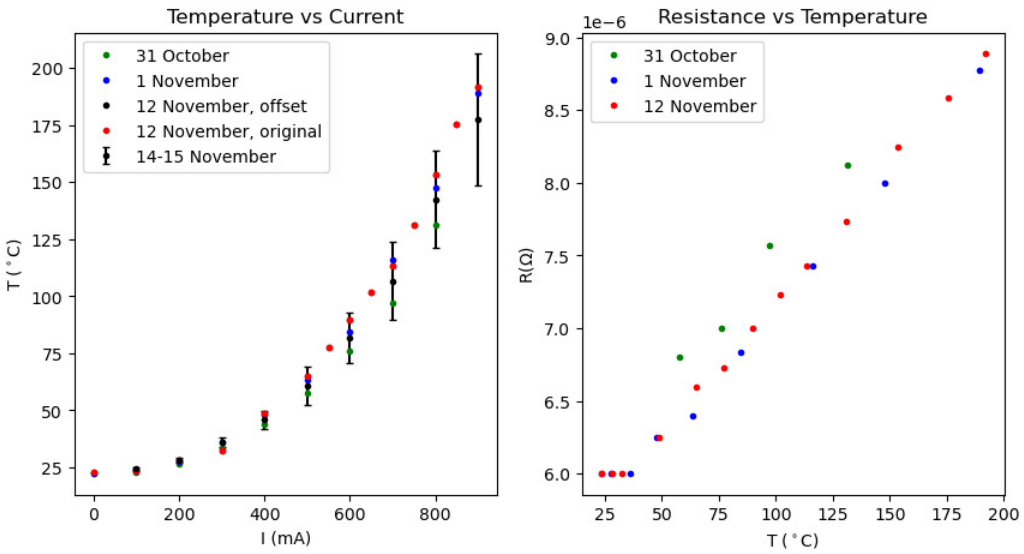

Figure 4.1: (L) The temperature of the tube increases nonlinearly with the current present in the wire. (R) Resistance of the wire increases with temperature.

also varies along the length of the tube. Second, there were complications in assembly of the V0.0 tube, including the wire snapping at one end and the need to leave a length of tube with no wire, as the V0.0 tube was not welded to a flange, meaning there were sections of the tube that were not heated.

Finally, human error is a marked factor in the variation. Because the temperature was measured by adjusting current in the wire and waiting until the thermocouple measurement stabilized before recording the temperature measured, there were decisions made as to how long to wait before making a measurement. These lengths of time were only recorded on 1 November. For the 1 November, 12 November, and 14–15 November data, time waited before recording temperature was consistent within the dataset (ranging from five to ten minutes across datasets), and for the 1 November and 12 November data, location of the thermocouple within the tube was also consistent. These data are also consistent with one another, indicating that the first and last sources of human error were successfully controlled.

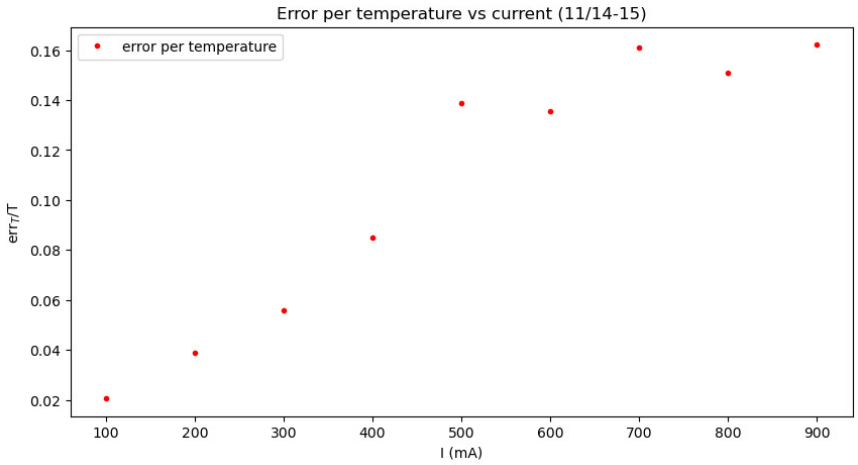

Figure 4.2: Relative error vs. current. Relative error is calculated from error range, which was taken on 11/14-15, and mean temperature across length for a given current.

The error indicated in Figure 4.1 resulted from measurements taken along the length of the tube in order to account for the first source of error described above. For each current, the temperature was measured at 1 cm, 2 cm, 3 cm, 4 cm, 5 cm, and 6 cm, as measured from the open end of the tube. The error bars visible in Figure 4.1 are the absolute range of that data. The error range per temperature is shown in Figure 4.2, which indicates a roughly linear relationship between current and relative error. This error data was taken on 14 November and 15 November. Since this source of error is due to manufacturing inconsistencies, a similar range of temperature is expected in the V1.0 and V2.0 designs. However, the temperature variation at the 120°C level is not enough to push the tube into a different effusive regime, and so is an acceptable variation.

The 12 November data was offset using variation in the thermocouple. Between each data point, the thermocouple was removed from the tube and used to measure the room temperature, then compared with a thermocouple that was only used for room temperature. This variation reached a maximum of 3.2 °C, and did not cause variation outside of the indicated error bars. The temperature measured on 31 October was

significantly reduced when compared to the temperature measured on all other dates, but still falls within the error bars as well. This error is likely due to either failure to wait sufficient time for the temperature to achieve a steady value, placement of the thermocouple at a different position within the tube than the other days, or both. Ultimately, this amounts to human error, while still being within an acceptable range of error.

Two further items of note became clear over the course of the testing of the sample tube, which may influence the status of the atomic beam source once assembly is completed. The first is that the epoxy underwent notable and reversible color changes (See Figure 4.3) when the wire had a relatively high current run through it (and therefore, at higher temperatures). This was first noted during the 1 November data collection, when the current present in the wire was 700 mA. Prior to data collection on 12 November, the author noted that the epoxy color had returned to its previous state. However, the color changed again while data was being collected. At this time, there are no expected impacts from this color change on the system, but the change is still of note.

The second item of note is that upon achieving high current/temperature ($T \approx 160$ °C), the author noticed a distinct smell coming from the assembly. It is unclear as to whether this smell originated from the epoxy, wire, tube, or the plastic insulator on the thermocouple wire. It is also unclear at which temperature the smell first begins to emerge, as the author was more focused on safety implications during the 1 November data collection (when the smell was first noted), and on 12 November through 15 November, the author was suffering from remaining symptoms of the flu which impacted their sense of smell. Regardless, the smell was notable at the 800 mA level and strengthened at 850 mA and 900 mA. This is notable because the smell indicates outgassing taking place somewhere within the tube-wire-epoxy assembly,

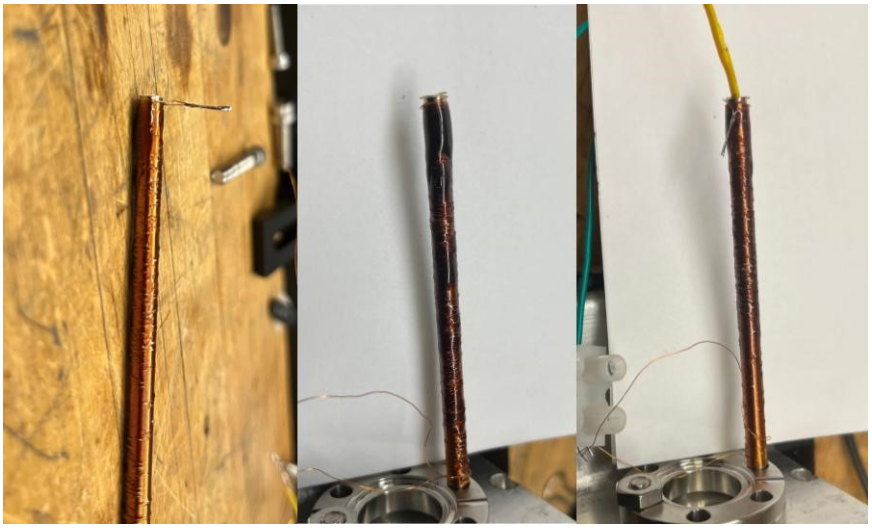

Figure 4.3: Epoxy color changes during temperature testing. (L) Image taken on 10/30. (C) Image taken on 11/14, after one hour of testing. (R) Image taken on 11/15, prior to testing.

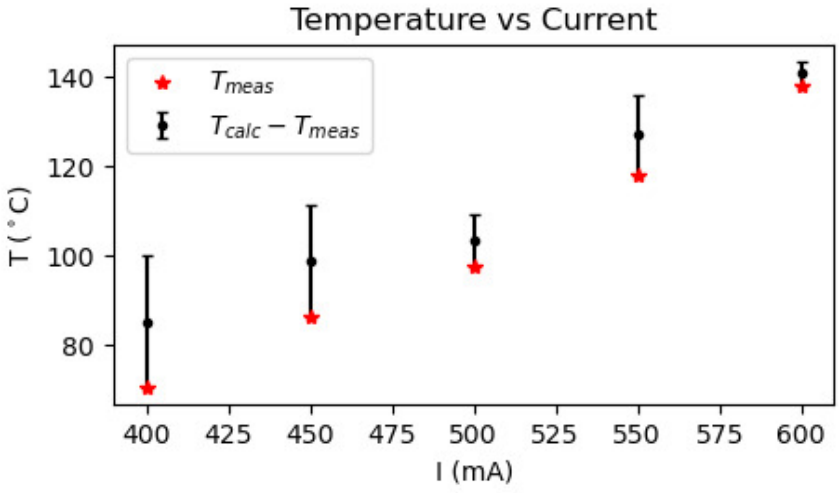

Figure 4.4: The temperature of the V1.0 tube increases roughly linearly with current. Predicted values of temperature from resistance using Equation 3.1 are indicated by use of error bars.

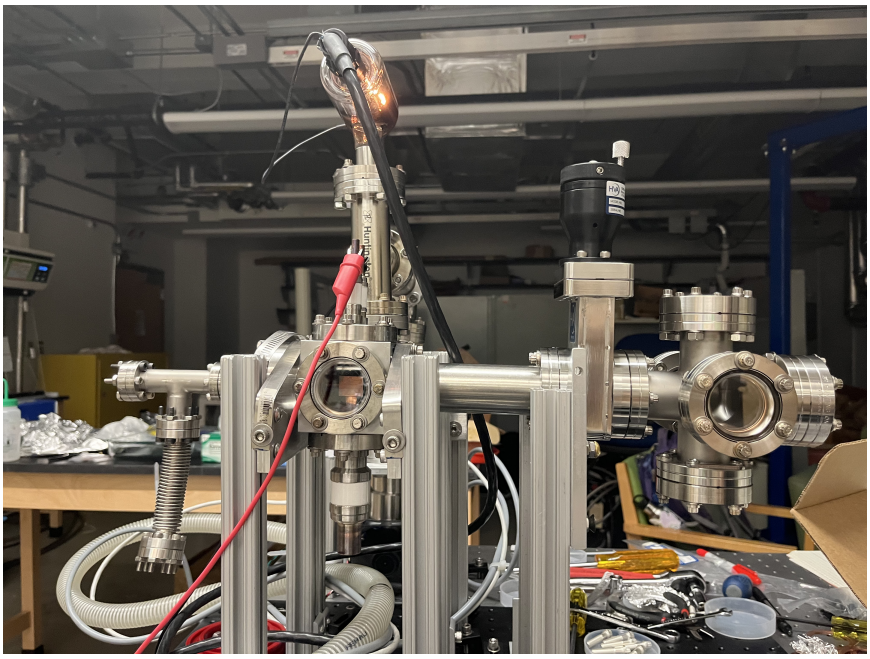

Figure 4.5: Full assembly of the beam apparatus with vacuum attachments and experimental chamber. The activated ion gauge may be seen at the center top. The experimental chamber consists of the 6-way cross to the right-hand side of the gate valve.

which has the potential to impact the achievable quality of vacuum.

Time constraints did not allow for a full dataset to be taken for the V1.0 beam regarding temperature of the collimation tube prior to vacuum appartus assembly, but data taken while the tube was outgassed indicated similar temperature distribution patterns as in the V0.0 tube. These results may be seen in Figure 4.4.

4.2 Assembly and Vacuum conditions

Pictured in Figure 4.5 is the most recent assembly of the beam portion of the apparatus (Figure 3.1) as of 21 April, 2025. A leak in the vacuum system was discovered when pumping down, allowing the system to reach a minimum of $2 \cdot 10^{-4}$ Torr rather than the anticipated 10^{-8} Torr. This leak was identified in the 2.75" diameter bellows connecting the Turbo pump to the rest of the system (pictured in the top left of Figure

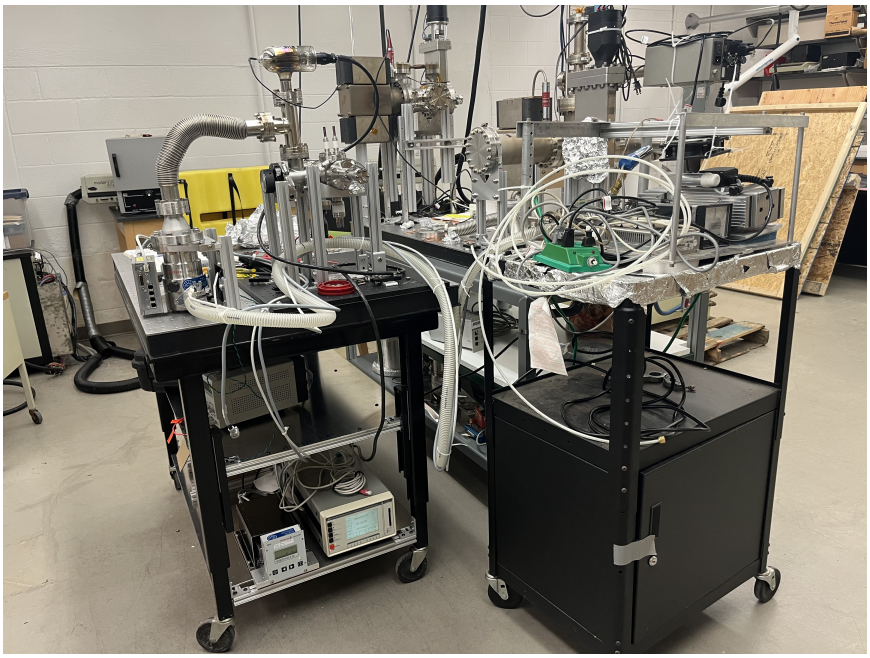

Figure 4.6: Full assembly of the beam portion of the apparatus with vacuum attachments. The Turbo pump may be seen in the bottom left, as well as a rough vacuum pump and gauge on the cart to the right.

4.6). This resulted in a second bellows needing to be washed and incorporated into the vacuum system, lengthening the assembly process. This leak was fixed, resulting in a minimum of $9 \cdot 10^{-8}$ Torr and allowing for pumping down of the main beam chamber. Vacuum pressure within the system was measured using an ion gauge, also pictured in the top left of Figure 4.6. Over the course of assembly, multiple sets of measurements were taken while perturbing the external surfaces of the apparatus in various ways in the effort to find any potential leak. This was done because, while the desired vacuum pressure for the completed apparatus is 10^{-7} to 10^{-6} Torr, the full apparatus (as opposed to the subsection connecting the Turbo pump to the angle valve and containing the ion gauge) was only able to achieve a minimum pressure of $1.3 \cdot 10^{-4}$ prior to leak-finding efforts. Three leak-finding and leak-fighting methods were used: application of small amounts of methanol to any joints or locations with leak potential; heating of individual components with a heat gun to remove any inter-

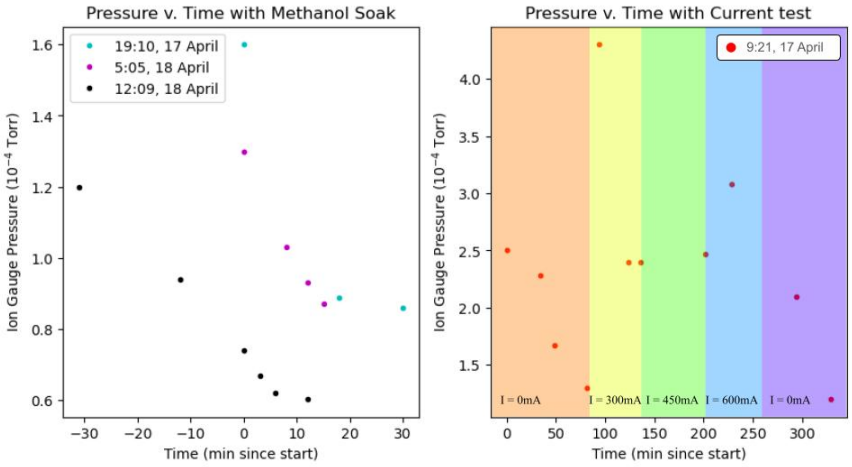

Figure 4.7: Vacuum pressure vs. time under different leak-finding methods. (Left) The impact of applying methanol to external vacuum components. The methanol was applied at minute 0 to the rubidium bellows (19:10 April 17) and the ceramic connections of the electrical feedthrough and copper rod feedthrough (5:05 April 18 and 12:09 April 18). (Right) The impact of applying current to the collimation tube on vacuum pressure. The colored regions are labeled with their current readings. The heat gun was simultaneously used on apparatus components, though this had no significant impact.

nal residue; and heating the collimation tube by running current through it to further outgas the epoxy. Ion gauge measurements while these measures were implemented may be seen in Figure 4.7.

Each dataset is labelled in Figure 4.7 by the time that the ion gauge was first activated. This is because the ion gauge, when first turned on, reads a higher vacuum pressure than is actually present and takes time (between 10 and 30 minutes) to drop its reading to the actual pressure present within the chamber. It is therefore expected that the pressure gradually drops, then approaches a plateau as time passes. No methanol was used for the 5:05, 18 April dataset, while methanol was applied to the ceramic seams of the electrical feedthrough and copper rod for the 19:10, 17 April and 12:09, 18 April datasets. The time of methanol application was normalized to $t = 0$ in the graph to illustrate the effects.

Expected results are that, if a leak was present, adding methanol would cause a sharp spike in ion gauge reading, then rapidly drop as the methanol freezes and seals the leak. The black points, the only dataset for which the gauge was allowed to drop prior to methanol application, shows no spike in pressure, but the pressure decreased faster after applying methanol. This is also shown by the other datasets, where the normal ion gauge drop (shown in magenta) has a more shallow slope than the cyan points, where the methanol effects were simultaneous with the ion gauge drop. At this time it is unclear what is causing this increased pressure drop rate, as no leak was detected.

The other expected source for pressure leakage is a virtual leak, or a component within the vacuum apparatus that is controlling the air rate such that the molecules cannot pass freely, slowing the pump-down process. Likely sources of virtual leaks include slow outgassing taking place within the epoxy used on the collimation tube, as well as in the unused open chamber of the ceramic standoff that faces the electrical feed-through flange. This chamber was partially sealed using epoxy, but because the epoxy is not entirely airtight, air escape is both possible and slow. There is also the possibility that the structure of the collimation tube itself is creating a virtual leak as collisions among air molecules traveling down the tube from the rubidium chamber prevent rapid evacuation. Heating the epoxy surrounding the collimation tube makes the outgassing process more rapid, so the tube was gradually heated to its operating temperature of 120 °C.

Ion gauge measurements were taken during this process, which may be seen in Figure 4.7. Here, time $t = 0$ indicates the time at which the ion gauge was activated, with the points in the leftmost $I = 0$ mA section showing the normal ion gauge drop. Raising the current to 300 mA and to 600 mA caused the expected pressure spike followed by a fall-off. However, the pressure did not spike as expected upon raising

the current from 300 mA to 450 mA. Finally, reducing the current back to 0 mA resulted in lower pressure than before the outgassing, though time constraints did not allow pressure to reach its minimum before the ion gauge had to be deactivated.

Over the course of this current test, data regarding voltage in the wire was also taken to confirm that temperature in vacuum could be calculated from resistance as anticipated. However, these measurements showed the voltage nearly two times smaller than expected; in atmosphere, temperature due to a 600 mA current in the wire caused a voltage of 5.9 V ($P = 3.54$ W), while the same current in the wire in vacuum only generated a voltage of 2.8 V ($P = 1.68$ W). This indicates that the temperature generated in the tube is smaller than anticipated due to lower power in the heater wire, though the underlying cause for this discrepency is unknown. This also may be a cause for the lack of spike in pressure when increasing from 300 mA to 450 mA. More research is needed to determine the cause for this voltage discrepancy and whether or not the temperature is impacted.

Final current tests with the intention of recreating this voltage discrepancy were performed on 24 and 25 April of 2025. The results of these tests may be seen in Figure 4.8. For low currents ($I \leq 300$ mA), the power exhibits a small, gradual increase over time. This corresponds with increases in resistance and voltage due to increasing temperature. Simultaneously, there is a slight "bump" in vacuum pressure that quickly returns to the "starting" level. Note that in the leftmost sections of Figure 4.8a and b, the ion gauge was still undergoing the normal pressure drop. For medium currents ($300 < I \leq 500$ mA), the 24 April measurements indicated a power and voltage drop after initially increasing. However, this did not recur when that same current range was tested on 25 April.

For high currents ($I \geq 600$ mA), the power and vacuum pressure gradually increased as time passed and current increased, before plateauing. However, when

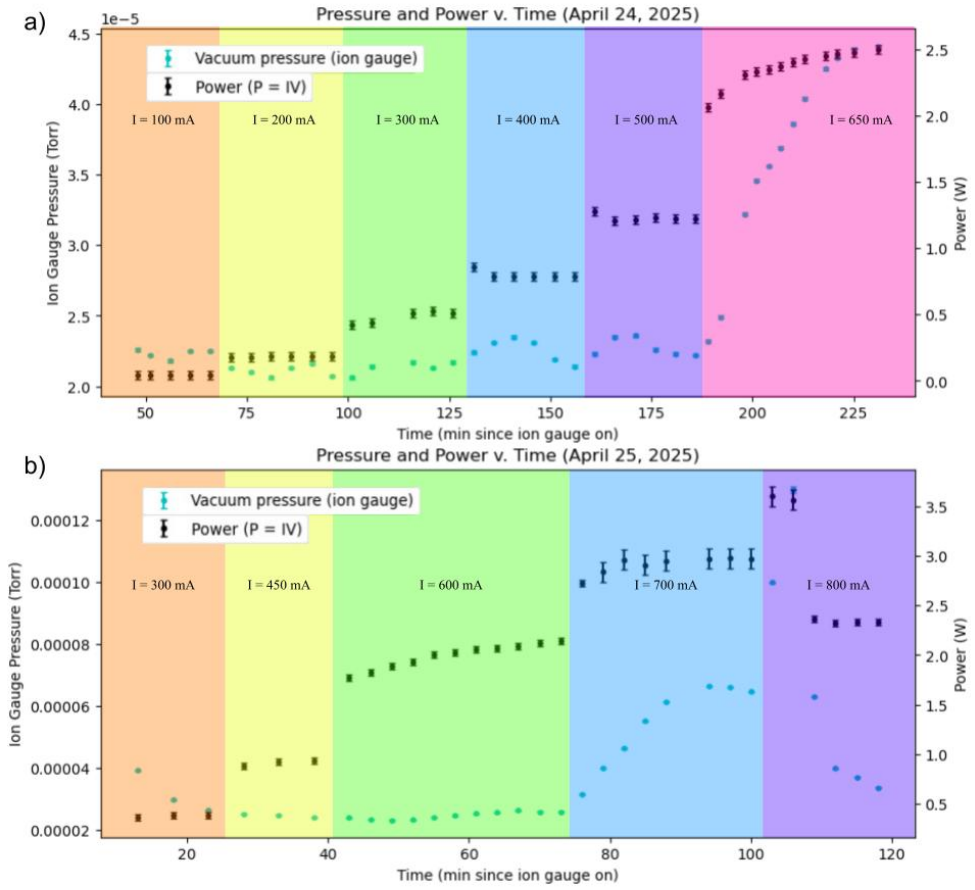

Figure 4.8: Vacuum pressure vs. time with increasing current. Time is in minutes since the ion gauge was turned on. The colored regions are labeled with current values for those data points.

current was raised to 800 mA, both voltage and vacuum pressure initially increased, then plummeted dramatically. The cause for this drop is unknown. Additionally, these results recreate the 17 and 18 April voltage discrepancy discussed above. It is possible that both the overall decrease in voltage and the sudden drop on 25 April are a result of contact between the copper wire and the conductive interior of the vacuum apparatus. This was confirmed by measuring non-infinite resistance between the electrical feedthrough prongs and the external walls of the apparatus using a multimeter. However, barring the unexpected failure of the wire insulation, the underlying cause of the contact is unclear. Further, this non-infinite resistance varied both depending on where on the apparatus the probes were placed and on which feedthrough prong was probed, indicating that the contact is closer to one prong than the other (and therefore, closer to one end of the wire).

Chapter 5

Conclusion and Outlook

Over the course of this thesis, final design and assembly methods for a rubidium atomic beam were devised. During and after apparatus assembly, testing of the temperature distribution and electrical behavior of the collimation tube created for the beam was conducted. This testing led to the conclusion that there is some form of contact between the copper wire wrapped about the collimation tube and the internal walls of the vacuum apparatus. This contact contributes to smaller resistance than expected in the collimation tube heater circuit, which in turn leads to lower temperatures in the wire than anticipated. Because of this, the fact that current in the vacuum apparatus walls would likely generate a non-zero magnetic field due to the non-uniform surface, and the fact that the achieved vacuum pressure was higher than desired, the beam apparatus was not activated and will be partially disassembled. The disassembly serves to diagnose the cause of the electrical contact and allows for replacement of the 1.33" spacer stack (see Figure 3.5) with the tapered nipple in Figure 3.7.

5.1 Future Experimentation

Further research is needed to determine the final beam characteristics of the apparatus built over the course of this project and draw final results and conclusions. Use

of a 780nm laser to analyze the D2 line of the rubidium in the beam is planned. The author was limited primarily by time constraints and the availability of materials, namely 2.75" copper gaskets, and thus was unable to complete this additional experimentation. Additionally, several parts experienced delays in arrival, including the gate valve that allowed the system to be partially pumped down without the initial presence of the experimental chamber. Further leaks in the initial vacuum apparatus delayed assembly completion significantly, leading to this lack of the intended experimental results. However, the atomic beam project is in a state where minor modifications should allow for the successful activation of the beam in the near future.

Once functional, the primary uses of the atomic beam by groups at the College of William & Mary will be for non-invasive probing of an electron beam and as a spectroscopic probe within a low-temperature plasma. In the short term, the atomic beam may also be used to form an atomic clock. Additionally, the vacuum apparatus was used by another College of William & Mary lab group to test the vacuum compatibility of a Langmuir probe to the 10^{-5} Torr level. Ultimately, the beam will be used as a source for a Zeeman slower to load a magneto-optical trap for ultracold atoms.

References

[1] P. Cren et al. "Loading of a cold atomic beam into a magnetic guide". In: *The European Physical Journal D* 20 (2002). DOI: https://doi.org/10.1140/epjd/e2002-00106-3.

[2] Giacinto Scoles. *Atomic and molecular beam sources*. Oxford University Press, 1987. ISBN: 978-0-195-04280-1.

[3] S. C. Bell et al. "A slow atom source using a collimated effusive oven and a single-layer variable pitch coil Zeeman slower". In: *Review of Scientific Instruments* 81 (2010). DOI: http://doi.org/10.1063/1.3276712.

[4] Y.-J. Lin et al. "Rapid production of ^{87}Rb Bose-Einstein condensates in a combined magnetic and optical potential". In: *Physical Review A* 79 (2009). DOI: https://doi.org/10.1103/PhysRevA.79.063631.

[5] Steinar H. W. Wouters et al. "Design and experimental validation of a compact collimated Knudsen source". In: *Review of Scientific Instruments* 87 (2016). DOI: http://doi.org/10.1063/1.4960997.

[6] C.B. Alcock. *Handbook of Chemistry and Physics*. 82nd ed. CRC Press LLC, 2001.

[7] C. B. Alcock, V. P. Itkin, and M. K. Horrigan. "Vapour Pressure Equations for the Metallic Elements: 298–2500K". In: *The Canadian Journal of Metallurgy and Materials Science* 23 (1984). DOI: https://doi.org/10.1179/cmq.1984.23.3.309.

[8] Dylan O. Sabulsky. "A Cesium-133 effusive oven for ultravold atomic experiments". B.A. Thesis. The University of Chicago, 2014.

[9] J. Ma et al. "Modification of glass cell walls by rubidium vapor". In: *Physical Review A* 79 (2009). DOI: https://doi.org/10.1103/PhysRevA.79.042905.

[10] Patrik Gádoros et al. "Laser cleaning and Raman analysis of the contamination on the optical window of a rubidium vapor cell". In: *Scientific Reports* 12 (2022). DOI: https://doi.org/10.1038/s41598-022-19645-z.

[11] Samuel Turner. "Research and design of an atomic beam source". Internal Report (unpublished). College of William & Mary, 2023.

[12] Samuel Turner. “Research and design of an atomic beam source”. Internal Report (unpublished). College of William & Mary, 2024.